AIAA JOURNAL
Vol. 47, No. 6, June 2009

Instantaneous Flame Anchor Measurements Behind a Rearward-Facing Step

A. A. Behrens,* J. M. Lutz,† and P. J. Strykowski‡
University of Minnesota, Minneapolis, Minnesota 55455

DOI: 10.2514/1.34643

The physical mechanisms governing flame anchoring have been examined in an effort to extend the range and maneuverability of compact, low-drag, air-breathing engines. Experiments were performed burning premixed methane and air in a planar dump combustor using reacting-flow particle image velocimetry as the primary diagnostic. Instantaneous two-dimensional images and vector fields were studied to determine changes in the fluid-chemical interactions of the shear layer as flame anchorability became more robust. Conditional averages of combustion products directed toward incoming reactants were evaluated to establish the connection to self-sustained combustion. A lean mixture of methane–air was used as a baseline, and the equivalence ratio and near-field counterflow were varied to affect anchorability. Dilatation was calculated as a marker for heat release and three-dimensionality. Operating points exhibiting a strong flux of products into reactants via a single coherent structure positioned downstream of the step were found to be most stable for flame anchoring. However, a counterflow level equal to 6.2% of the primary stream by mass was found to match the characteristics of a single coherent structure while maintaining multiple structures in the mixing zone, effectively increasing heat release rates at a lower equivalence ratio.

Introduction

RAMJET propulsion systems will require improvements in operability to become more useful technologies. Currently, ramjet engines operate successfully over a very narrow range of conditions, greatly limiting maneuverability, range, speed, fuel type, and consumption rates [1,2]. Without turbocompression, scramjet and ramjet engines must operate at high velocities using ram compression to achieve high pressures within the combustor. At these high velocities, the residence times within the combustor are short, on the order of a millisecond in a ramjet, and typically insufficient to fully combust most hydrocarbon fuels. To sustain a flame, highly reactive fuels, such as hydrogen, with high flame speeds are needed and must be stabilized by a flame holder, typically a bluff body. Unfortunately, these fuels are extremely volatile compared with common hydrocarbon jet fuels, which are readily accessible and easily stored.

To achieve maximum range and maneuverability, the combustion process must be stable and sustained over a wide operating domain with minimal associated drag. This is inherently difficult; to sustain combustion, flames are anchored by a low-speed zone created by a bluff body [3,4]. Examples of bluff bodies include v gutters, cavities, and sudden expansions, all of which are plagued by high drag for the very reason they are conducive to flame anchoring: they create flow separation and reverse flow. The flame anchor geometry is also closely linked to the ability to sustain combustion; therefore, simply reducing flame anchor size to reduce drag is not a suitable strategy as it narrows the range of operability [3,4]. Thus, short combustion residence times and high drag due to stagnation pressure loss behind bluff body flame anchors are problems that hinder ramjet and scramjet engine performance.

Detailed information obtained in the near field of the flame anchor will lead to a better understanding of the sustained combustion and turbulent flame characteristics vital to improvement in flame anchor design. The following experiments were designed to move away from blowout conditions via multiple paths, exploring the mechanisms responsible for sustained combustion. The baseline case was positioned as close to the lean blowout limit as possible while still maintaining a stable flame. Flames were further stabilized by independently increasing the equivalence ratio and the level of counterflow employed near the trailing edge. The detailed conditions downstream of the step responsible for flame stabilization were examined by superimposing the instantaneous flame on the velocity-vector fields. Conditional averages of product gases directed toward the incoming premixed reactants were also used to assist in interpreting conditions for flame stability.

Flame Anchor Theory

A main goal of this research is to gain a more detailed understanding of the physical mechanisms governing flame anchoring behind bluff bodies. Previous research has studied the role of parameters such as geometry, pressure, temperature, and inlet velocity on flame sustainability, creating blowout criteria based on these quantities determined a priori [3–9]. A key result was the stability criteria based on mean operating values as summarized by Frolov et al. [9]: $U/(p^{\alpha}H^{\beta}T^{\gamma}) = f(\phi)$, with parameters U, p, H, and T representing inlet velocity, combustion chamber pressure, length scale of the bluff body, and inlet temperature. Various studies have provided a range of exponent values for α, β, and γ given by Frolov [9]. The resulting physical interpretation of Frolov's expression is that greater flame stability occurs for combustors with large flame anchors operating at high temperatures, high pressures, and low velocities. Bluff bodies are successful flame anchors owing to the separated flow set up when the reactants move past the body. The recirculation zone behind the bluff body supplies combustion radicals with enough energy to overcome the activation energy of incoming reactants, thus initiating burning within the shear layer where instabilities assist in flame surface convolution. Higher inlet temperatures increase flame anchorability because more combustion radicals have sufficient energy to overcome the activation energy requirement for initiating combustion. Higher pressures increase

Received 17 September 2007; revision received 2 February 2009; accepted for publication 16 February 2009.

*Graduate Research Assistant, Department of Mechanical Engineering, 111 Church Street Southeast.

†Graduate Research Assistant, Department of Mechanical Engineering, 111 Church Street Southeast; currently, Aerothermal engineer, Aero Systems Engineering, 358 East Fillmore Avenue, St. Paul, Minnesota 55107.

‡Professor, Department of Mechanical Engineering. Senior Member AIAA.

contact between combustion radicals and reactants. Reduced inlet velocity allows fluid packets following a trajectory into the recirculation zone enough time to fully convert to products as they circulate and are injected back into the reactant stream. Whereas previous research has gained a general knowledge based on mean operating conditions [3–9], a more fundamental understanding of flame anchoring is considered in this work by examining the instantaneous fluid-chemical interactions behind a bluff body created by a backward-facing step.

This study focuses on the mechanisms sustaining combustion that lie within the instantaneous fluctuations of mass and energy in the shear layer along the boundary of the recirculation zone. Figure 1 shows, schematically, the flux of high-temperature products pertinent for flame stability. The capability of a fluid packet to participate in the ignition of new reactants at a fixed position in the shear layer is dependent on a number of parameters. The fluid packet requires a sizeable volume, to avoid conduction losses, with a high-enough temperature to overcome the activation energy of the fuel. Additionally, the packet must contain reaction-initiating radicals of hot combustion products to continue to ignite incoming reactants. The packet velocity must be directed toward the flame with sufficient velocity to penetrate into the reactant field, but with a low strain rate to avoid tearing the flame. Thus, the more fluid packets with the appropriate set of conditions to initiate reactions, the more robust the flame anchor.

Flame Anchor Measurements

This research was focused on examining two-dimensional instantaneous planes of the reacting flowfield to locate and study positions within the shear layer containing combustion products directed toward incoming reactants. The goal was to provide insight into the regions along the shear layer that promote sustained combustion. The inlet velocity and laminar flame speed were varied to determine the physical changes within the shear layer as blowout was approached. Countercurrent shear control has been observed in previous studies to aid flame stability and to extend the lean operating limit; therefore, its role was also examined [10–13].

Particle image velocimetry (PIV) was used to obtain the instantaneous velocities and provide a mapping of the reactant and product fields. Reacting flow PIV was implemented by seeding the primary flow of premixed fuel/air with aluminum oxide particles of a nominal size of 0.5 μm. According to Stella et al. [14], a 0.5 μm aluminum oxide particle will follow a flow up to an 80 kHz oscillation, which is well within the typically selected cutoff frequency of 10 kHz chosen for reacting flows [14,15]. The seed particles have a melting point of 2300 K and therefore will not participate in the chemical reactions [16]. A Continuum, Inc., Nd:Yag laser produced two thin coplanar light sheets at 532 nm with up to a 230 mJ/pulse capability. The laser sheets were directed into the combustor via a quartz window along a transverse-streamwise plane near the midpoint of the span. A Kodak MegaPlus camera with two 1008×1018 pixel charge-coupled device arrays was positioned perpendicular to the light sheet to capture laser light scattered off particles through a second quartz window. The camera captures two images of particle fields separated by roughly 25 μs in conjunction with the pulses of the two coplanar laser sheets. A narrow band filter (532 nm) was used to filter out ambient light and flame luminosity. The software packages Insight 3G by TSI, Inc., and ProVision-XS by Integrated Design Tools, Inc. (IDT), were used to spatially cross correlate small interrogation regions of the larger image; the IDT package was particularly helpful when interrogating the images and deducing velocities across the flame front.

One necessary condition for sustained combustion, as described earlier, is a consistent flux of high-temperature products into the approaching reactant stream. To identify critical locations along the shear layer where this flux occurs, the regions within the product gases having positive vertical velocity, that is, those directed into the reactant stream, were marked. Figure 2 shows a representative instantaneous image acquired immediately downstream of the backward-facing step for an inlet velocity of 9 m/s at an equivalence ratio of $\phi = 0.78$. Note that the product region contains a lower particle density caused by the appreciable drop in gas density across the flame front when high-temperature products are formed. Because the reactant region is saturated with aluminum oxide particles, pixel values in the reactant region are of greater intensity, providing a convenient binary marker for the temperature field and a means to quantify the flame location.

A region immediately downstream of the step where product gases possess substantial vertical velocities has been identified in Fig. 2. When examining instantaneous velocity fields, we have used the vertical velocity of the products to assess locations along the flame where product flux leads to effective flame anchoring. Conditional averages of the vertical velocity and gas temperature were taken over 300–500 instantaneous PIV images to highlight product flux at a given operating condition and spatial location along the flame front.

To identify the flame location, the images were broken into small 16×16 pixel interrogation regions (physical dimension of 0.7 mm per side) from which the average pixel intensity was determined. A threshold was selected as the cutoff between the reactants and the products based upon this average pixel intensity; the rather-distinct interface led to consistent predictions of flame location over a range of intensity cutoffs. The flame obtained in this manner can be seen superposed on top of the image in Fig. 2 (as well as the figures to follow). The velocity field was evaluated using ProVision-XS with a 32×32 pixel interrogation window and 50% overlap, thereby matching a velocity vector with its average pixel intensity for each interrogation region throughout the particle image. The vertical velocity was normalized by the inlet reactant velocity, U_R, at each operating point.

Experimental Facilities

Experiments were conducted using premixed methane and air in a modified single-sided dump combustor. The combustion facility consists of a methane introduction assembly, seeding apparatus, and a combustor rig. The combustor test section, as shown in Fig. 1, is supplied by reactants issuing from a rectangular section of height H and depth $8H$ into an expansion of 2:1, where the step height $D = H$. The combustor length downstream of the step was equal to $10H$ and issued into an exhaust duct at atmospheric pressure; the reference frame for all measurements is taken congruent with the step. The boundary layer upstream of the step had a thickness of $0.1H$ and an

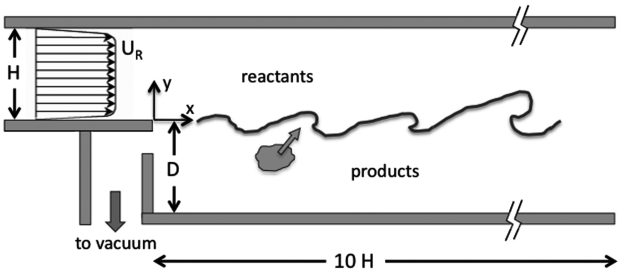

Fig. 1 Experimental configuration of planar single-sided dump combustor.

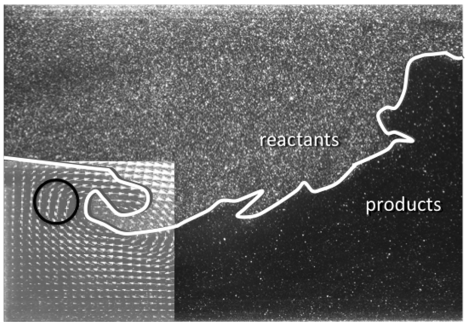

Fig. 2 Instantaneous particle image with flame interface identified. Product gases within circled region have strong reactant-directed velocities.

rms turbulence level (based in the streamwise velocity component) of approximately 8–10% of the average reactant velocity U_R. A vacuum chamber is connected to a pump that pulls a secondary flow from the combustor, creating counterflow near the trailing edge. In the absence of counterflow, the gap in the rearward-facing plate is sealed. The reader is referred to Behrens and Strykowski [10] for a more detailed combustor geometry as well as facility and instrumentation setup.

The mixture of methane and air entered the combustor with mean velocities ranging from 9 to 12 m/s. These velocities correspond to Reynolds numbers based on step height from 1.1 to 1.4×10^4. Hot-wire measurements determined core turbulence levels in the reactant stream to be less than 2% of its mean velocity. For equivalence ratios of 0.6–0.78, the overall heat release rate of the combustor ranged from 70 to 90 kW. A high-voltage arc was positioned in the low-speed zone behind the rearward-facing step to act as an ignition source; the igniter was engaged until a flame was present and then it was subsequently removed from the combustor.

Countercurrent shear flow control was implemented in a similar manner to previous studies [10–13,17]. The basic premise of the control is to enhance the naturally occurring countercurrent shear flow in a typical dump combustor. As the reactants enter a traditional step combustor, flow separates over the backward-facing step. This induces a velocity profile in the region of recirculation similar to that of a countercurrent shear layer. The goal of the control scheme is to further enhance the natural profile of the baseline combustor by increasing the reverse flow within the recirculation zone. This is accomplished by creating a pressure sink via a vacuum positioned behind the step. Creating a stronger secondary flow in the vicinity of the trailing edge has been shown by Forliti and Strykowski [17] to affect turbulent production and strain rates, important parameters for robust turbulent combustion.

Results

A baseline case was chosen near the lean limit, which exhibited characteristics of flame anchoring on the verge of failing. This baseline choice was made so that the changes in the fluid-chemical interactions would be most apparent when operating conditions with robust flame anchors were studied. New operating points were created by increasing the equivalence ratio ϕ and the amount of counterflow (measured as a percent of mass flow relative to the reactant stream) for comparison with the baseline case. The cases tested, as well as the baseline conditions, are summarized Table 1.

Baseline

Flame anchoring characteristics were examined for a baseline condition at an inlet velocity of 11.6 m/s and an equivalence ratio of $\phi = 0.60$. The baseline condition was chosen by mapping the general performance of the facility to identify the lean limit. The mapping began at an equivalence ratio chosen below the lean burning limit, and the flame characteristics were closely monitored as the equivalence ratio was increased. Initially the flame was unstable and prone to blowout. Further increases of the equivalence ratio to nearly $\phi = 0.60$ resulted in a flame that was self-sustaining upon removal of the igniter. This stable burning near the lean limit without the igniter was defined as the baseline case.

To examine the flowfield and flame dynamics at each operating condition, hundreds of instantaneous PIV images were studied. This procedure was facilitated by creating movies of each flow condition

Table 1 Baseline and test cases used to examine flame anchor characteristics

	ϕ	U_R (m/s)	counterflow, % of primary	Flame stability
Baseline	0.60	11.6	0	At lean limit
Case I	0.73	11.7	0	Stable
Case II	0.78	9.0	0	Very stable
Case III	0.60	11.6	3–8%	Variable

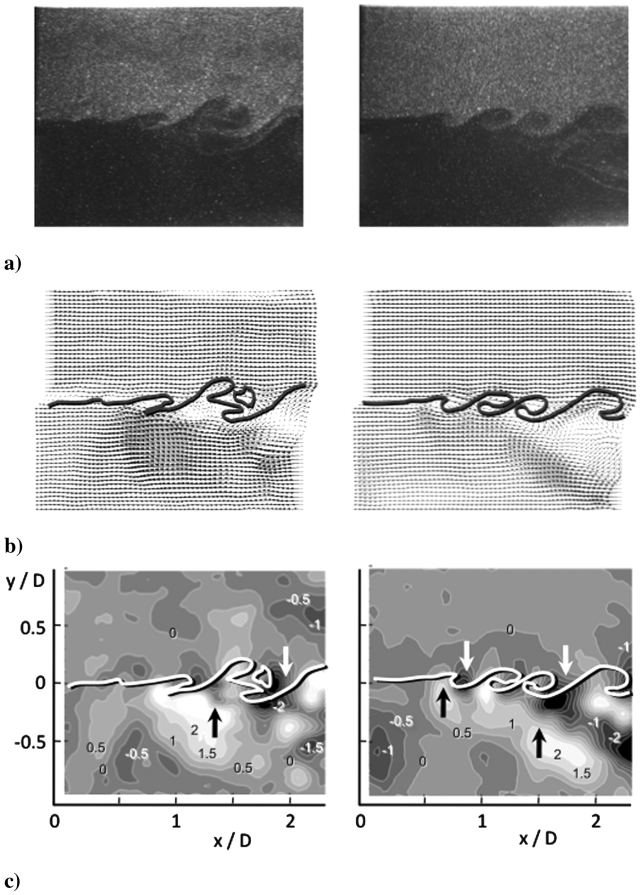

Fig. 3 Instantaneous flow features for baseline conditions (U_R= 11.6 m/s, $\phi = 0.60$): a) particle images, b) velocity-vector fields with superimposed flame interface, and c) isocontours of the vertical-velocity component.

built from individual snapshots of particle images, velocity-vector fields, and contours of the flame-directed (i.e. vertical) velocities. Figure 3 reveals two random snapshots of these images for the baseline case. Each set of images corresponds to a field of view of approximately x/D between 0 and 2.3 and $y/D = \pm 0.95$. The upper images of Fig. 3 illustrate the distinct concentration interface between premixed reactants and products created by gas expansion across the flame. Although gray areas make precise flame location somewhat ambiguous in its fine detail, the contrast is sufficiently robust to consistently identify the primary flame features algorithmically as discussed earlier; these flame interfaces were overlaid on the velocity vector and contour plots as shown in Figs. 3b and 3c and used in the movie files to interpret flame behavior. (The approach described herein was also used in the interpretation of Figs. 4–6 to follow.)

To assist in the identification of flow structure, a convective velocity, approximately equal to one-third of the incoming reactant mean velocity, was subtracted from the velocity-vector fields. The term "flow structure" is used qualitatively in the present context and corresponds to our interpretation of the approximate lateral and cross-stream dimensions of fluid elements in the product and reactant streams. Observations were aided by the effective shading in velocity-vector fields in Fig. 3b and the vertical-velocity contours identified in Fig. 3c, as well as the superimposed instantaneous flame sheet. Quantification of the flow structures in the flame zone is provided by way of conditional averages described in the sections to follow.

The baseline flow is distinguished by multiple small-scale structures formed in the mixing region downstream of the step. The structures have comparable positive and negative vertical velocities; the contour levels in Fig. 3c indicate the magnitude of the vertical-velocity component and range between ± 2 m/s or, equivalently,

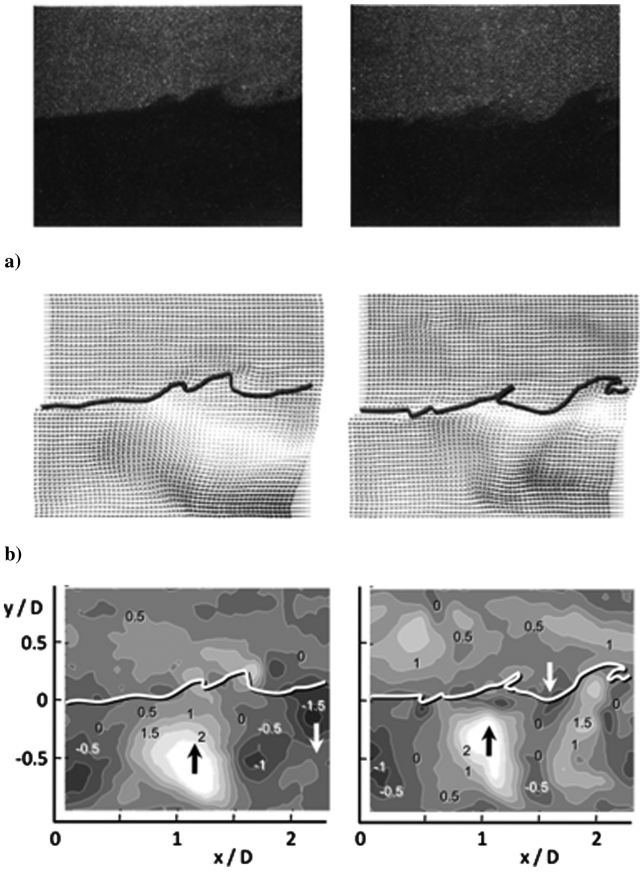

Fig. 4 Instantaneous flow features for case I ($U_R = 11.7$ m/s, $\phi = 0.73$): a) particle images, b) velocity-vector fields with superimposed flame interface, and c) isocontours of the vertical-velocity component.

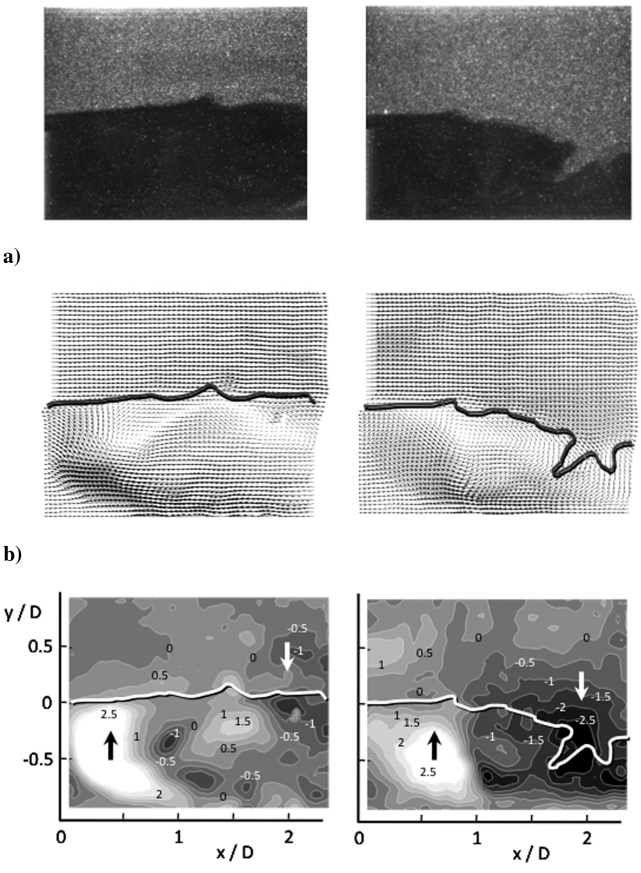

Fig. 5 Instantaneous flow features for case II ($U_R = 9.0$ m/s, $\phi = 0.78$): a) particle images, b) velocity-vector fields with superimposed flame interface, and c) isocontours of the vertical-velocity component.

$\pm 17\%$ of the incoming reactant stream. The structures have dimensions of approximately $1/4D$ in the downstream portion of the interrogation region; outside the narrow mixing region, the flow appears relatively undisturbed, which will be important when comparing to the cases examined in the subsequent discussion. The small-scale structures grow in the streamwise direction along the separation plane; their scale and magnitude are consistent image to image and lead to concomitant flame wrinkling. The comparison of vertical velocities and flame wrinkling in Fig. 3c is particularly helpful in understanding how the flow disturbances impact the flame development. The arrows in the figure are used to emphasize locations along the shear layer showing consistent upward flow of products or downward flow of reactants.

Equivalence Ratio

To enhance flame stability, the equivalence ratio was raised from 0.60 to 0.73 by increasing the mass flow of methane without altering the valve settings to the primary airstream. This resulted in a very subtle increase in the total mass flow rate to the burner, corresponding to an average reactant velocity of 11.7 m/s, that is, an increase of less than 0.9% from the baseline of 11.6 m/s. This decision was made to avoid resetting the primary airstream, which had a slightly higher uncertainty from run to run.

Representative particle images, vector fields (convective reference frame), and vertical-velocity plots are shown for the higher equivalence ratio, case I, in Fig. 4. The burning process at $\phi = 0.73$ is differentiated from the baseline case by the tendency to form one large structure in the product region with a scale of $\sim 1/2D$. The single nominally stationary structure resided at the streamwise location of $x/D \sim 1$ and was associated with a strong vertical velocity originating deep within the product gases. Unlike the observations in Fig. 3, small-scale structures do not appear to persist in the immediate neighborhood of the flame, nor in the reactant gases, suggesting that the heat release at the flame front is effectively suppressing shear layer instabilities and flame wrinkling.

The enhanced flame stability at the increased equivalence ratio is attributed to the formation of the larger structure in the product gases. The increased momentum of products toward the approaching reactant stream at $x/D \sim 1$ creates a consistent transport of reaction-initiating radicals. The flame sheets observed in Fig. 4 are substantially less convoluted than those seen in the baseline case. In part, this is a consequence of the single large coherent structure residing further away from the reactant–product interface. Research conducted on the effects of heat release in turbulent-free shear flows [18–20] has shown that increased heat release suppresses shear layer instabilities, thereby reducing entrainment and flame convolution, and causes a shift to larger integral scales.

As predicted by Frolov et al. [9], an increase in the equivalence ratio will result in stronger flame anchors, but unfortunately this also can create unstable combustion. The presence of a nominally two-dimensional structure in the recirculation zone occurring at increased ϕ can lead, through feedback, to thermoacoustic instability. To examine this phenomenon in the present facility, we increased the equivalence ratio at a constant forward velocity, but were unable to establish conditions associated with thermoacoustic instability, identified by the presence of large pressure oscillations. However, by reducing the forward velocity to 9.0 m/s, we were able to achieve thermoacoustic instability at $\phi \sim 0.8$. Hence, we set our facility for case II to $U_R = 9.0$ m/s and $\phi = 0.78$ to examine a strong flame anchor just before the onset of instability.

Figure 5 shows the burning results for case II. Similar to case I (Fig. 4) and in contrast to the baseline case (Fig. 3), one large structure dominates the mixing zone and has a transverse scale of

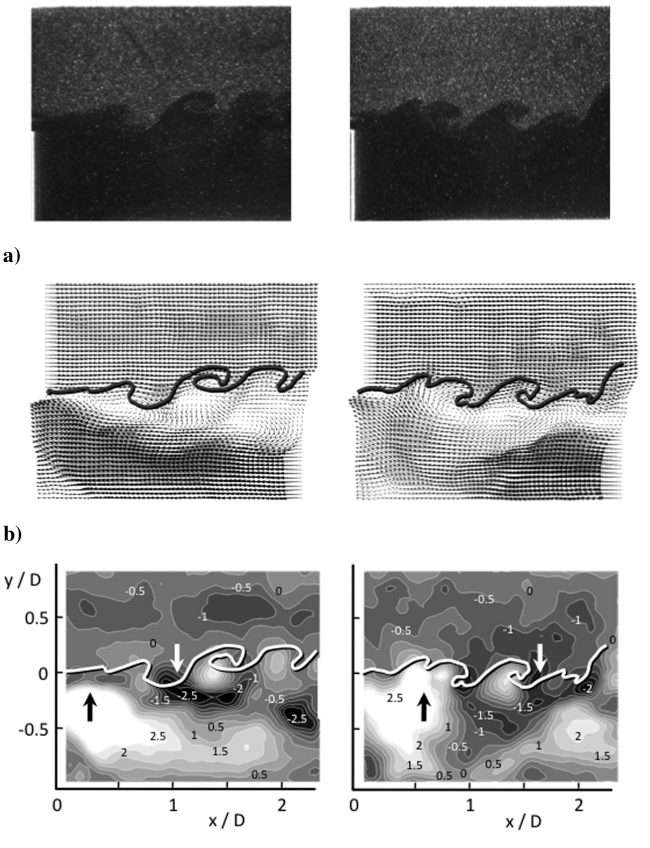

Fig. 6 Instantaneous flow features for case III at 6.2% counterflow ($U_R = 11.6$ m/s, $\phi = 0.60$): a) particle images, b) velocity-vector fields with superimposed flame interface, and c) isocontours of the vertical-velocity component.

order of $3/4D$ and a lateral scale of approximately twice that. The presence of a single large structure generates a volume of products directed toward reactants with a vertical velocity of nearly 30% of U_R, which acts as a very strong mechanism for flame anchoring. As can be seen from the particle images, the flame contours of case II show a dramatic decrease in flame wrinkling compared with the baseline case. The flame sheet is seen, in the vector fields, to reside on top of the main structure. Note that the movement of the structure upstream to $x/D \sim 0.5$ allows the observation of a strong downward-directed flow of reactants at $x/D \sim 2$; at times, the flame is seen to wrap around the downstream side of the structure, bringing the flame in close proximity to the lower combustor wall. It is the pressure rise caused by the rapid disintegration of this structure upon its interaction with the wall that is commonly associated with thermoacoustic instability.

Counterflow Control

Counterflow control has been employed recently in the dump combustor environment with the aim of increasing volumetric heat release rates without increasing the equivalence ratio [10–13,17]. The control is established by enhancing the reverse velocity in the recirculation zone, created by a vacuum source positioned directly below the trailing edge. Enhanced countercurrent shear in the present geometry has been studied under isothermal conditions [17] and has been shown to create large flow structures and introduce turbulent kinetic energy into a relatively large spectral band. In reacting environments, the control has been shown to extend the lean burning limit as well as increase the stability of the flame anchor [10–13]. By exploring the flame anchor using PIV, the current study provides insight into the augmentation of the fluid-chemical interactions created by countercurrent shear control, which are responsible for enhanced flame anchorability.

The control studies were conducted at the same operating point as the baseline case: an inlet velocity of 11.6 m/s and an equivalence ratio of $\phi = 0.60$. Three levels of counterflow control were tested, identified by the amount of mass pulled via suction out of the combustor as a percentage of the inlet mass flow rate. The levels of suction mass flow tested were 1) low, 3.7%; 2) medium, 6.2%; and 3) high, 7.6%.

Figure 6 shows representative snapshots taken at 6.2% counterflow. In comparison to the baseline case (Fig. 3), the vector and vertical-velocity plots of Figs. 6b and 6c reveal a substantially more convoluted flame interface, particularly in the shear layer upstream of $x/D \sim 1$; the scale of the structures impacting the flame are also observed to be larger with counterflow. Furthermore, the counterflow leads to a consistently strong upward flow of products in the neighborhood of the trailing edge (~17–22% of the reactant velocity), somewhat reminiscent of the behavior observed at higher equivalence ratios in case II ($U_R = 9.0$ m/s and $\phi = 0.78$; see Fig. 5) and known to be important for a robust flame anchor. The benefits of counterflow [10–13,17] observed elsewhere, including an increase in integral length scale, increased turbulent kinetic energy, and elevated heat release rates, are borne out qualitatively in Fig. 6. The counterflow case exhibits stronger upward and downward flux of products and reactants, which are distributed more uniformly along the shear layer. As quantitative measures will show in the next section, a reliable source of product gases directed toward the flame with kinetic-energy-carrying flow structures is essential for a robust flame anchor.

Flame Anchor Measurements

To develop criteria for flame anchorability based on the experimental observations of increased flux of product gases into reactants, conditional averages of the vertical flux of products V_P were computed; the vertical velocities were averaged over 300–500 images. A filter was used to select vertical velocities between 7 and 65% of the inlet velocity, to keep out possible erroneous vectors on the low side confounded by the PIV resolution and on the high side given that vertical velocities greater than 65% were statistical outliers.

We are interested in capturing the average locations along the flame front where high-temperature products will likely impact the flame zone. Conditional averages of V_P were obtained at various horizontal planes below the separation plane at $y = 0$. Planes too close to the flame were compromised by flame intersection (and the associated biasing by reactants), and planes too far removed from the shear layer were thought to provide less reliable insight into products ultimately impacting the flame zone. The plane at $y/D = -0.25$ was selected as a compromise between those limits.

Figure 7 shows the magnitude of the conditional-averaged vertical velocities for the baseline case and cases I and II; for clarity, the counterflow cases are graphed separately in Fig. 8. A maximum product velocity is observed for the baseline case at 9% of the mean inlet velocity, whereas a maxima of 15 and 22% are reached for cases I and II, respectively. The increased vertical velocities over the baseline case are a result of the strong pumping mechanism developed by the formation of a single vortex with an increasing equivalence ratio. Particularly for cases I and II, in which the peaks in the conditional average are quite distinct, the streamwise location of the peak and its magnitude correspond quite well with the observations in the instantaneous images of Figs. 4 and 5, suggesting that the flow structure residing in the products is rather stationary. The region of maximum vertical velocity is also observed to shift upstream with increasing ϕ as seen in the instantaneous flow. The shift upstream and narrowing of the peak of the product flux is indicative of the increased coherence of a single structure in the products. This coherence can lead to the formation of thermoacoustic instabilities, thus rendering these operating points less desirable despite the development of a robust flame anchor [20–22].

Countercurrent flow near the trailing edge has been used to reduce the likelihood of thermoacoustic instability by enhancing the three dimensionality of the shear layer in the neighborhood of the step

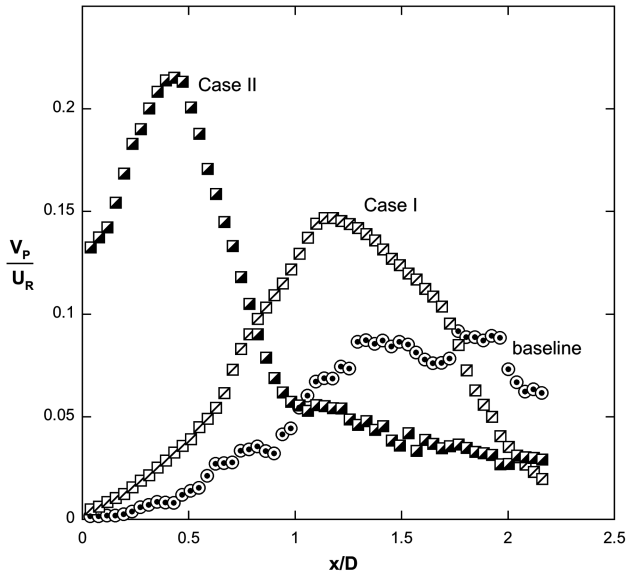

Fig. 7 Conditional-averaged vertical velocities obtained in the product gases at $y/D = -0.25$ for cases I and II.

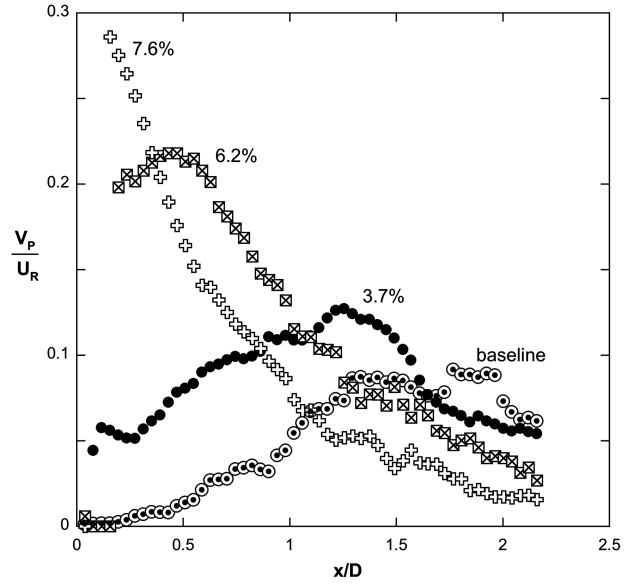

Fig. 8 Conditional-averaged vertical velocities obtained in the product gases at $y/D = -0.25$ for case III.

[10,17]. In the current study, the flame anchor was stabilized by counterflow levels of 3.7 and 6.2%, but at the highest level of counterflow the flame had a tendency to blow out. The flux of products for the counterflow cases is shown in Fig. 8. The maximum vertical velocity increases in magnitude and moves upstream toward the step for elevated levels of counterflow. Interestingly, the least stable flame anchor at 7.6% counterflow shows a strong upward flow of products near the trailing edge. However, velocity-vector fields reveal that, at 7.6% counterflow, a fraction of the product gases are drawn along the rearward-facing step and out of the combustor through the vacuum system and, hence, do not participate in the ignition process. The intermediate level of counterflow of 6.2% does, however, correspond to a stable flame, as it is able to enhance recirculation of product gases away from the trailing edge. The difference between the two cases is that, at 7.6% counterflow, the product gases with a vertical momentum sufficient to penetrate the incoming reactants are drawn out of the combustor; at 6.2% counterflow, the products removed from the combustor by the vacuum system do not contain the highest momentum fluid, allowing it to interact with reactants and assist in the ignition process slightly downstream of the trailing edge.

A comparison of the most stable flame anchors in our study, case II and the counterflow study at 6.2%, reveal very similar distributions of V_P within the combustor. The 6.2% counterflow operating condition reaches a peak in product flux at $x/D \sim 0.5$, which is coincident with the low speed and high equivalence ratio of case II. The magnitude of the maximum flux of the two is also comparable, at approximately 22%. However, the product flux is more laterally distributed in the combustor with counterflow; for example, at $x/D = 1$ the product flux with counterflow is over 10% of U_R, which is approximately double that of case II at the same streamwise position. Hence, with counterflow, there is a larger region within the shear layer downstream of the step, which is also producing upward movement of hot products to promote burning.

Although a stable flame anchor is critical for robust combustor performance, we are also interested in those conditions that can increase high volumetric heat release rates at lean equivalence ratios. Furthermore, stable burning is often disrupted in dump-type geometries by thermoacoustic instabilities that occur when organized structures within the combustor, modulated by the inherent acoustic modes of the facility, become coherent and two dimensional. The organized structures are eventually broken up by impingement with the combustor wall, upon which they burn rapidly, causing a spike in pressure. When amplified by inherent acoustic modes, pressure magnitudes can become great enough to cause mechanical damage and blowout. Stable operating points need to be strongly three dimensional to prevent a coupling of acoustic and pressure waves within the combustor.

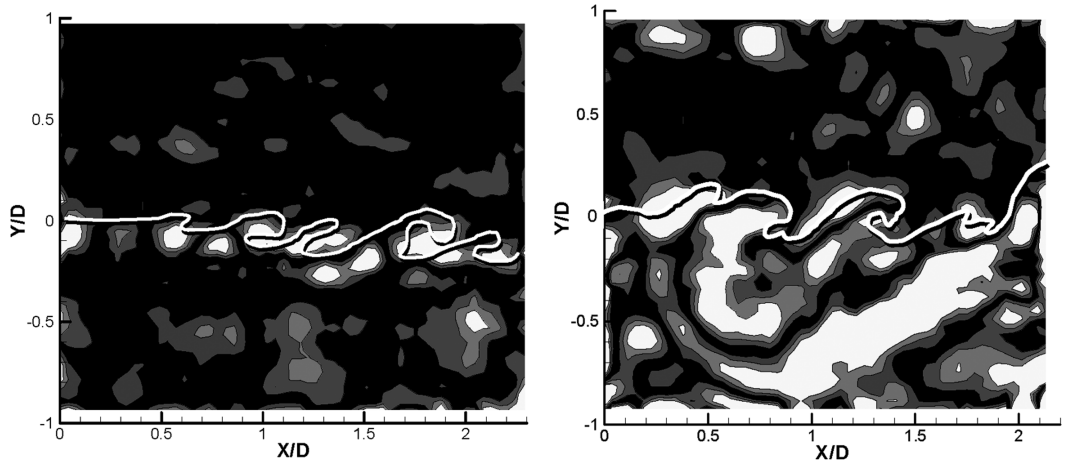

Fig. 9 Representative dilatation contours with flame sheet superimposed. Dilatation increases in magnitude from dark to light.

Figures 5 and 6 indicate that, despite comparable levels of product flux at $x/D \sim 0.5$, the flame is substantially more wrinkled in the combustor with counterflow. To understand the origin of this flame distortion, the three dimensionality in the flowfield was quantified using dilatation, defined as $\Delta \equiv |\partial u/\partial x + \partial v/\partial y|$; note that dilatation has also been shown by Mungal et al. [23] to be an effective marker for flame position. Figure 9 shows examples of two-dimensional dilatation contours with superimposed flame sheets, highlighting the ability of Δ to mark both heat release and three dimensionality; the dark areas correspond to $\Delta = 0$, namely, two-dimensional constant density flow. In Fig. 9a (baseline conditions), the light areas only occur near the flame contour where heat release would be expected, whereas, in Fig. 9b (counterflow at 6.2%), light areas also occur well below the flame sheet due to the presence of three dimensionality in the product gases.

Dilatation in the products was averaged between $y/D = -0.95$ (slightly above the lower combustor wall) and the flame sheet to assess the integrated effect of heat release and three dimensionality for the flow conditions studied. As observed in Fig. 10, the disturbance level in the product gases for cases I and II is comparable to the baseline conditions; three dimensionality increases in the streamwise direction as the shear layer grows spatially. As expected, the increased heat release rates with increases in the equivalence ratio are the consequence of higher flame temperatures rather than increased flame surface area. The impact of counterflow on flow three dimensionality (at a fixed equivalence ratio) can also be observed in Fig. 10. Dilatation increases monotonically with the level of counterflow and appears to saturate near $x/D \sim 2$.

The advection of products into the flame zone (quantified by V_P/U_R), together with accompanying flow disturbances marked by Δ, assists in flame wrinkling and augmentation of heat release rates due to increased flame surface area. The algorithm employed to mark the flame interface was also used to integrate the distance along the flame; the length of the interface was normalized by the lateral extent of the PIV domain (x/D between 0 and 2), providing a measure of the flame length relative to a flat laminar flame originating at the step. Figure 11 shows the normalized flame length as a function of counterflow level; the inset provides the flame length dependence on the equivalence ratio (the data were averaged over 300 realizations). At the baseline conditions, the flame is approximately 50% greater than a flat flame sheet and decreases by approximately 10% when the equivalence ratio is increased (cases I and II), in agreement with previous research indicating that higher flame temperatures shift structures to larger length scales and less wrinkled flames [18–20]. As counterflow is applied, the structures advected into the flame are more intense, leading to flame convolution and, therefore, increased heat release rates. The overall increase in flame length, as well as the dilatation with counterflow control, provides a quantification of previous observations, that is, an increase in flame wrinkling leads to increased volumetric heat release rates and strong flow three dimensionality [10].

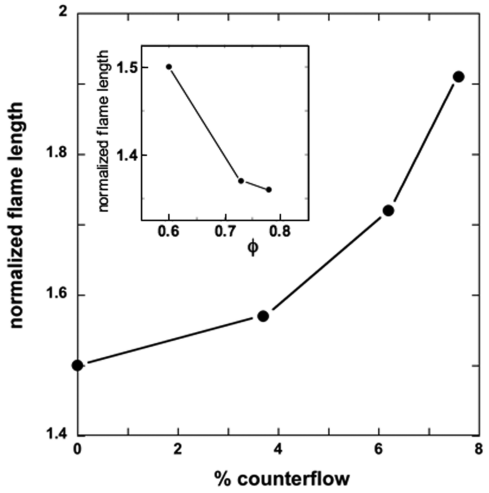

Fig. 11 Average flame length as a function of equivalence ratio (inset) and percent counterflow.

A number of features have been discussed that create a desirable operating condition: a robust flame anchor, three dimensionality promoting increased volumetric heat release, and a decreased tendency toward thermoacoustic instabilities. In an effort to identify optimal conditions for combustion, that is, a robust flame anchor with the potential for high heat release rates, these effects were combined. The product flux V_P/U_R measured along the horizontal plane at $y/D = -0.25$ was multiplied with the average dilatation $\bar{\Delta}$ at the same streamwise location; the dilatation was normalized by its magnitude for the baseline case. The results are shown in Fig. 12 for the two most stable flame anchors in our study and compared with the marginally stable flame at the baseline conditions. The baseline conditions suffer from the combination of an inconsistent flux of products and the absence of flame-wrinkling structures in the very near field of the step; the flux-dilatation product reflects these observations. The flame anchor most susceptible to thermoacoustic instability, case II, provides strong product flux for flame anchoring, but the absence of disturbances advected into the flame to disrupt the strong two-dimensional character of the flame.

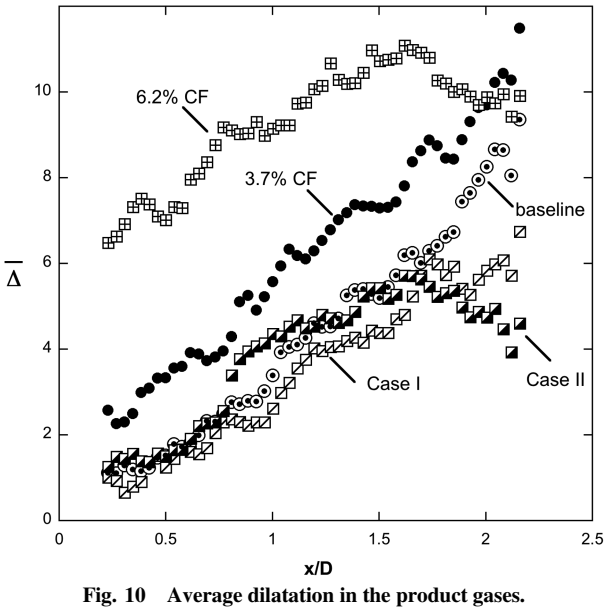

Fig. 10 Average dilatation in the product gases.

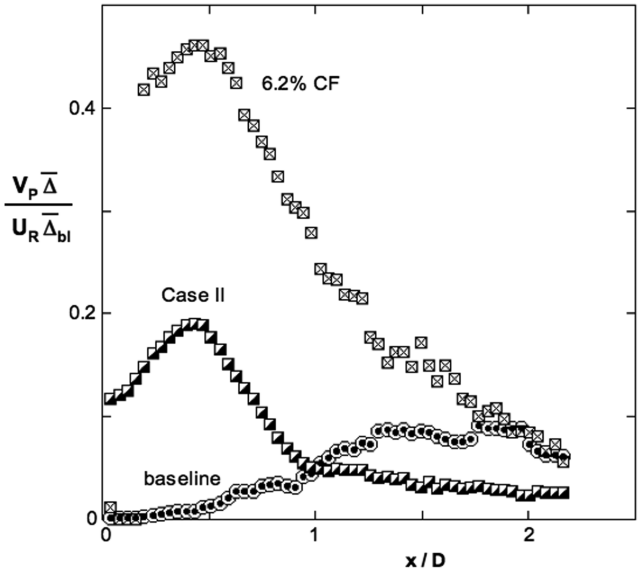

Fig. 12 Dilatation-velocity product obtained in the region below the flame.

Case II shows a clear peak at $x/D \sim 0.5$. However, the narrow peak indicates that there is a fairly small streamwise region that experiences a strong positive vertical flow of fluid and must be countered by a similarly strong downward flow to maintain mass continuity within the recirculation zone. By contrast, the counterflow case shown in Fig. 12 shows that significant advection of disturbed product gases occurs along a sizeable portion of the shear layer, providing for strong flame anchoring and flame convolution and capable of achieving higher heat release rates at leaner equivalence ratios.

Conclusions

The physical mechanisms governing flame anchoring were examined in more detail to gain a better understanding of the criteria for self-sustained combustion. Several operating points were chosen to study how conditions in the shear layer changed as flame anchoring became more robust. Reacting flow PIV was used to obtain instantaneous measurements of velocity and temperature within the flowfield downstream of the step and also to mark the instantaneous flame surface. Conditional averages of hot product gases directed toward the incoming reactant stream were computed to gain insight into the physiochemical conditions along the shear layer conducive for stable flame anchors.

Countercurrent control provides a practical option for increasing the stability of the flame anchor while operating at higher combustor throughputs and leaner burning limits. It has the added benefit of increasing flame anchorability without the formation of large coherent structures, as was the case with increasing the fuel flow rate. The coherent structures of the other two test cases produced large updrafts of products, which sustain burning, but are a contributing factor to the formation of thermoacoustic instabilities. Counterflow control allowed for flow three dimensionality while strengthening flame anchorability and robust burning by amplifying mixing intensity.

Acknowledgments

This research would not have been possible without the financial support of the Office of Naval Research, contract N00014-05-1-0253, and the guidance we have received from our technical monitor, Gabriel D. Roy.

References

[1] Fry, R. S., "A Century of Ramjet Propulsion Technology Evolution," *Journal of Propulsion and Power*, Vol. 20, No. 1, 2004, pp. 27–58. doi:10.2514/1.9178

[2] Keller, J. O., Vaneveld, L., Korschelt, D., Hubbard, G. L., Ghoniem, A. F., Daily, J. W., and Oppenheim, A. K., "Mechanism of Instabilities in Turbulent Combustion Leading to Flashback," *AIAA Journal*, Vol. 20, No. 2, 1982, pp. 254–262. doi:10.2514/3.51073

[3] Williams, G. C., Hottel, H. C., and Scurlock, A. C., "Flame Stabilization and Propagation in High Velocity Gas Streams," *Third Symposium (International) on Combustion and Flame*, The Williams & Wilkins Co., Baltimore, MD, 1949, pp. 21–40.

[4] Spalding, D. B., "Theoretical Aspects of Flame Stabilization," *Aircraft Engineering and Aerospace Technology*, Vol. 25, 1953, pp. 264–276.

[5] Zukoski, E. E., and Marble, F. E., "Experiments Concerning the Mechanism of Flame Blow-Off from Bluff-Bodies," *Proceedings of the Gas Dynamics Symposium on Aerothermochemistry*, Northwestern Univ., Evanston, IL, 1956, pp. 205–210.

[6] Plee, S. L., and Mellor, A. M., "Characteristic Time Correlation for Lean Blowoff of Bluff-Body-Stabilized Flames," *Combustion and Flame*, Vol. 35, 1979, pp. 61–80. doi:10.1016/0010-2180(79)90007-5

[7] De Champlain, J. A., and Bardon, M. F., "A Model for Bluff Body Flame Stabilization," American Society of Mechanical Engineers Paper 86-GT-155, June 1986.

[8] Kundu, K. M., Banerjee, D., and Bhaduri, D., "On Flame Stabilization by Bluff-Bodies," *Journal of Engineering for Power*, Vol. 102, 1980, pp. 209–214.

[9] Frolov, S. M., Basevich, V. Ya., and Belyaev, A. A., "Mechanism of Turbulent Flame Stabilization on a Bluff-Body," *Chemical Physics Reports*, Vol. 18, No. 8, 2000, pp. 1495–1516.

[10] Behrens, A. A., and Strykowski, P. J.,"Controlling Volumetric Heat Release Rates in a Dump Combustor Using Countercurrent Shear," *AIAA Journal*, Vol. 45, No. 6, 2007, pp. 1317–1323. doi:10.2514/1.24059

[11] Behrens, A. A., Hallberg, M. P., Forliti, D. J., and Strykowski, P. J., "Control of a Backward-Facing Step Combustor Employing Suction at the Dump Plane," *Proceedings of the 16th Office of Naval Research Propulsion Conference*, Univ. of Southern California, Los Angeles, CA, June 2003, pp. 208–213.

[12] Behrens, A. A., Anderson, M. J., and Strykowski, P. J., "PIV Measurements in a Premixed JP10/Air Dump Combustor: Role of Counterflow on Turbulence and Heat Release," *Proceedings of the 18th Office of Naval Research Propulsion Conference*, Naval Postgraduate School, Monterey, CA, Aug. 2005, pp. 143–148.

[13] Behrens, A. A., "Reacting Flow Studies in a Dump Combustor: Enhanced Volumetric Heat Release Rates and Flame Anchorability," Ph.D. Thesis, Univ. of Minnesota, Minneapolis, MN, Dec. 2006.

[14] Stella, A., Guj, G., Kompenhans, J., Raffel, M., and Richard, H., "Application of Particle Image Velocimetry to Combusting Flows: Design Considerations and Uncertainty Assessment," *Experiments in Fluids*, Vol. 30, No. 2, 2001, pp. 167–180. doi:10.1007/s003480000151

[15] Melling, A., "Tracer Particles and Seeding For Particle Image Velocimetry," *Measurement Science and Technology*, Vol. 8, No. 12, 1997, pp. 1406–1416. doi:10.1088/0957-0233/8/12/005

[16] Ancimer, R., Wallace, J., and Jaaskelainen, H., "Investigations into the Effect of LDV Seed Particles on the Operating Characteristics of a Spark Ignition Engine," *Experiments in Fluids*, Vol. 27, No. 2, 1999, pp. 175–180. doi:10.1007/s003480050342

[17] Forliti, D. J., and Strykowski, P. J., "Controlling Turbulence in a Rearward-Facing Step Combustor Using Countercurrent Shear," *Journal of Fluids Engineering*, Vol. 127, No. 3, 2005, pp. 438–448. doi:10.1115/1.1899170

[18] Hermanson, J. C., and Dimotakis, P. E., "Effects of Heat Release in a Turbulent Reacting Shear Layer," *Journal of Fluid Mechanics*, Vol. 199, 1989, pp. 333–375. doi:10.1017/S0022112089000406

[19] McMurtry, P. A., Riley, J. J., and Metcalfe, R. W., "Effects of Heat Release on the Large-Scale Structure in Turbulent Mixing Layers," *Journal of Fluid Mechanics*, Vol. 199, 1989, pp. 297–332. doi:10.1017/S002211208900039X

[20] Hermanson, J. C., Mungal, M. G., and Dimotakis, P. E., "Heat Release Effects on Shear-Layer Growth and Entrainment," *AIAA Journal*, Vol. 25, No. 4, 1987, pp. 578–583. doi:10.2514/3.9666

[21] Pitz, R. W., and Daily, J. W., "Combustion in a Turbulent Mixing Layer Formed at a Rearward-Facing Step," *AIAA Journal*, Vol. 21, No. 11, 1983, pp. 1565–1570. doi:10.2514/3.8290

[22] Gabruk, R. S., and Roe, L. A., "Velocity Characteristics of Reacting and Nonreacting Flows in a Dump Combustor," *Journal of Propulsion and Power*, Vol. 10, No. 2, 1994, pp. 148–154. doi:10.2514/3.23723

[23] Mungal, M. G., Lourenco, L. M., and Krothapalli, A., "Instantaneous Velocity Measurements in Laminar and Turbulent Premixed Flames Using On-Line PIV," *Combustion Science and Technology*, Vol. 106, 1995, pp. 239–265. doi:10.1080/00102209508907781

R. Lucht
Associate Editor